Nuclear Science and Techniques (2023) 34:30
https://doi.org/10.1007/s41365-023-01178-3

Systematic study of proton radioactivity half-lives

Yang-Yang Xu[1] · Xiao-Yuan Hu[1] · De-Xing Zhu[1] · Xi-Jun Wu[2] · Peng-Cheng Chu[3] · Xiao-Hua Li[1,4,5,6]

Received: 14 October 2022 / Revised: 20 December 2022 / Accepted: 21 December 2022 / Published online: 28 February 2023

Abstract

In the present study, on the basis of the screened electrostatic effect of the Coulomb potential, we propose an improved Gamow model within the centrifugal potential in which there are only two adjustable parameters, i.e., the screened parameters t and g, which represent the combined effect of the interaction potential and reduced mass of the emitted proton-daughter nucleus on the half-life of proton radioactivity in the overlapping region. Using this model, we systematically calculated the proton radioactivity half-lives of 31 spherical nuclei and 13 deformed nuclei and obtained corresponding root-mean-square deviations of 0.274 and 0.367, respectively. The relationship between the proton radioactivity half-life of $^{177}\mathrm{Tl}^{m}$ and the corresponding angular momentum l removed by the emitted proton is also discussed. In addition, we used the proposed model to predict the proton radioactivity half-lives of 18 nuclei whose proton radioactivity is energetically allowed or observed but not yet quantified in NUBASE2020. For comparison, we used the universal decay law of proton radioactivity proposed by Qi et al. (Phys Rev C 85:011303, 2012. https://doi.org/10.1103/PhysRevC.85.011303), and the new Geiger–Nuttall law of proton radioactivity proposed by Chen et al. (Eur Phys J 55:214, 2019. https://doi.org/10.1140/epja/i2019-12927-7).

Keywords Proton radioactivity · Gamow model · Half-lives

1 Introduction

Proton radioactivity, i.e., the disintegration of nuclei by emitting a proton and the formation of a new nuclide, is a typical decay mode for odd-Z emitters beyond the proton drip line, which represents a fundamental limit of nuclear existence where the nuclei spontaneously shed off excess protons to stabilize. This phenomenon was first discovered in 1970 by Jackson et al. from a high-spin isomer $^{53}\mathrm{Co}^{m}$ [1, 2] and independently confirmed by Hofmann et al. and

This work was supported in part by the National Natural Science Foundation of China (Nos. 12175100 and 11975132), the Construct Program of the Key Discipline in Hunan Province, the Research Foundation of Education Bureau of Hunan Province, China (Nos. 21B0402 and 18A237), the Natural Science Foundation of Hunan Province, China (No. 2018JJ2321), the Innovation Group of Nuclear and Particle Physics in USC, the Shandong Province Natural Science Foundation, China (No. ZR2022JQ04), the Hunan Provincial Innovation Foundation For Postgraduate (No. CX20220993), and the Opening Project of Cooperative Innovation Center for Nuclear Fuel Cycle Technology and Equipment, University of South China (No. 2019KFZ10).

✉ Xiao-Hua Li
lixiaohuaphysics@126.com

Xi-Jun Wu
wuxijun1980@yahoo.cn

Peng-Cheng Chu
kyois@126.com

1 School of Nuclear Science and Technology, University of South China, Hengyang 421001, China

2 School of Math and Physics, University of South China, Hengyang 421001, China

3 The Research Center for Theoretical Physics, Science School, Qingdao University of Technology, Qingdao 266033, China

4 National Exemplary Base for International Science and Technology. Collaboration of Nuclear Energy and Nuclear Safety, University of South China, Hengyang 421001, China

5 Cooperative Innovation Center for Nuclear Fuel Cycle Technology and Equipment, University of South China, Hengyang 421001, China

6 Key Laboratory of Low Dimensional Quantum Structures and Quantum Control, Hunan Normal University, Changsha 410081, China

Klepper et al. from ground states of ^{151}Lu [3] and ^{147}Tm [4] in 1982. Since then, proton radioactivity has attracted wide attention in the nuclear physics community [5–19] because it can provide crucial information of neutron-deficient nuclei, such as their shell structure [20] and the coupling between bound and unbound nuclear states [21]. Moreover, as the inverse process of rapid proton capture, it can contribute significantly to the understanding of element origin and star evolution [22].

With the development of experimental facilities and technology, new nuclei undergoing proton radioactivity have been discovered. So far, there are approximately 45 proton emitters with $51 \leq Z \leq 83$ detected [23–26], 15 of which are in isomeric state and the remaining are in ground state. We can also divide them into approximately 32 spherical nuclei and 13 deformed nuclei, according to the degree of deformation. Theoretically, proton radioactivity obeys the quantum tunnel theory, i.e., a proton tunnels through a potential barrier between the emitted proton and daughter nucleus, which is the same decay mechanism as α decay. Based on this description, a great number of models, microscopic approaches, and empirical formulas have been proposed to analyze this process, such as the effective interaction potential model of density dependent M3Y (DDM3Y) [27], distorted-wave Born approximation (DWBA) [28], Lejeune and Mahaux (JLM) [29], coupled-channels approach (CCA) [30–32], unified fission model (UFM) [33, 34], two-potential approach (TPA) [35], generalized liquid drop model (GLDM) [36–38], single fold model (SFM) [39], Coulomb and proximity potential model (CPPM) [40], universal decay law of proton radioactivity (UDLP) [41], and new Geiger-Nuttall law of proton radioactivity (NG-N) [42], among others. These studies have greatly advanced our understanding of proton radioactivity and are still evolving.

In 2005, based on the Gamow model and considering the overlapping effect, Tavares et al. first proposed the one-parameter model (OPM) to study the α decay of bismuth isotopes with an angular momentum l=5 removed by the emitted α particle [43]. Subsequently, OPM was applied to evaluate the α decay half-lives of platinum, neptunium, and uranium isotopes, with the calculated results being in good agreement with the experimental data [44–46]. Recently, Zou et al. successfully generalized OPM to favored proton radioactivity based on the same mechanism of tunneling effect [47]. For proton radioactivity, an odd proton must penetrate a barrier containing nuclear, Coulomb, and centrifugal potentials. Compared with α and cluster decays, the centrifugal potential plays a more important role in proton radioactivity because protons have less mass than α particles and clusters. In addition, the probability of protons penetrating the barrier is sensitive to the value of the outer turning point, i.e., the right-most intersection of the decay energy and proton-daughter nucleus interaction potential. When the Coulomb potential is replaced by the Hulthen potential [48], the screened effect shifts the outer turning point to the left [49, 50]. Thus, it is crucial to consider the contribution of the centrifugal potential and screened electrostatic effect when analyzing proton radioactivity. To this end, based on the Gamow model, we systematically studied proton radioactivity by jointly considering the screened electrostatic effect and centrifugal potential together with experimental data from the latest table of evaluated nuclear properties, i.e., NUBASE2020 [51].

The remainder of this paper is organized as. In Sect. 2, the theoretical frameworks for the calculation of proton radioactivity half-life and screened electrostatic barrier are described in detail. The calculations and discussion are presented in Sect. 3. Finally, Sect. 4 provides a brief summary.

2 Theoretical frameworks

The proton radioactivity half-life is generally defined as

$$T_{1/2} = \frac{\ln 2}{\lambda} = \frac{\ln 2}{\nu_0 S_p P_{se}}, \tag{1}$$

where λ is the proton radioactivity constant depending on the collision frequency of the emitted proton in the potential barrier ν_0, the spectroscopic factor S_p (probability of finding the daughter nucleus with a certain state J^π in the mother nucleus), and the penetrability factor P_{se} (probability of a proton penetrating through the external barrier); ν_0 can be calculated as

$$\nu_0 = \frac{\omega}{2\pi} = \frac{(2n_r + l + 3/2)\hbar}{2\pi \mu_0 {R_n}^2} = \frac{(G + 3/2)\hbar}{1.2\pi \mu_0 {R_0}^2}. \tag{2}$$

Here, ω is the oscillation frequency [52] and μ_0 denotes the reduced mass between the emitted proton and daughter nucleus in the final decaying nuclear system. In this study, the nucleus root-mean-square (rms) radius R_n was estimated as ${R_n}^2$=$3/5{R_0}^2$ [53], where $R_0 = 1.240 A_p^{1/3}(1 + 1.616/A_p - 0.191(A_p - 2Z_p)/A_p)$, with A_p and Z_p being the mass and proton number of the parent nucleus, respectively. $G = 2n_r + l$ is the principal quantum number, where n_r and l are the radial and angular momentum quantum numbers, respectively; $\hbar$ denotes the reduced Planck constant.

Spectroscopic factor S_p and penetrability factor P_{se} are defined as follows:

$$S_p = e^{-G_{ov}}, G_{ov} = \frac{2}{\hbar}\int_a^b \sqrt{2\mu_{ov}[V_{ov}(r) - Q_p]}dr,$$
$$P_{se} = e^{-G_{se}}, G_{se} = \frac{2}{\hbar}\int_b^c \sqrt{2\mu_{se}[V_{se}(r) - Q_p]}dr. \quad (3)$$

Here, G_{ov} and G_{se} are the Gamow factors in the overlapping ($a \sim b$) and separating ($b \sim c$) regions, as shown in Fig. 1; μ_{ov}, μ_{se}, V_{ov}, and V_{se} are the reduced mass and interaction potential in the overlapping and separating regions, respectively; Q_p is the energy released by proton radioactivity. In Fig. 1. a and b denote the inner turning point and separating point, respectively; their values are equal to $R_p - R_{proton}$ and $R_d + R_{proton}$. $R_{proton} = 0.8409$ fm is the radius of the proton, obtained from Ref. [54]. R_p and R_d are the radii of the parent and daughter nuclei, respectively. They were calculated using the droplet model of an atomic nucleus; detailed calculations can be found in Ref. [57]. Finally, c is the outer turning point of the potential barrier that satisfies the condition $V(c) = Q_p$. μ_0 and Q_p can be calculated as

$$\frac{1}{\mu_0} = \frac{1}{m_d} + \frac{1}{m_{proton}}, \quad (4)$$

$$m_d = A_d + \frac{\Delta M_d}{F} - \left(Z_d m_e - \frac{10^{-6}kZ_d{}^{\beta}}{F}\right), \quad (5)$$

$$Q_p = \Delta M_p - (\Delta M_d + \Delta M_{proton}) + 10^{-6}k(Z_p{}^{\beta} - Z_d{}^{\beta})\,\text{MeV}. \quad (6)$$

Here, m, A, Z, and ΔM are the atomic mass, mass number, proton number, and mass excess, respectively, and the subscripts p, d, e, and proton represent the parent nucleus, daughter nucleus, electron, and proton, respectively. F = 931.494009 MeV/u is the mass-energy conversion factor. The quantity kZ^{β} is the total binding energy of the Z electrons in the atom, whereas the term $k(Z_p{}^{\beta} - Z_d{}^{\beta})$ represents the screened effect of the atomic electrons. For $Z \geq 60$, k = 8.7 eV and β=2.517, while for $Z < 60$, k=13.6 eV and β =2.408; these values were derived from data reported by Huang et al. [58]. In addition, $V(r)$ denotes the total interaction potential between the emitted proton and daughter nucleus, which is sketched in Fig. 1.

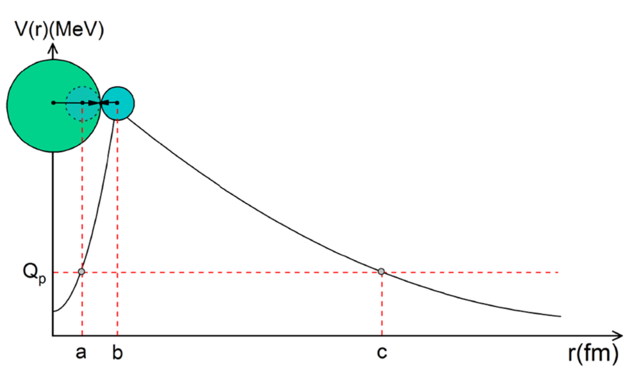

Fig. 1 (Color online) Schematic diagram of proton-daughter nucleus interaction potential $V(r)$

Generally, in the process of proton radioactivity, the total interaction potential $V(r)$ between the emitted proton and daughter nucleus consists of the nuclear potential $V_n(r)$, Coulomb potential $V_c(r)$, and centrifugal potential $V_l(r)$. It is expressed as

$$V(r) = V_n(r) + V_c(r) + V_l(r). \quad (7)$$

Here, the centrifugal potential $V_l(r)$ is written as

$$V_l(r) = \frac{(l + 1/2)^2\hbar^2}{2\mu_0 r^2}, \quad (8)$$

where the minimum angular momentum l_{min} removed by the emitted proton is calculated as

$$l_{min} = \begin{cases} \Delta_j, & \text{for even } \Delta_j \text{ and } \pi_p = \pi_d, \\ \Delta_j + 1, & \text{for even } \Delta_j \text{ and } \pi_p \neq \pi_d, \\ \Delta_j, & \text{for odd } \Delta_j \text{ and } \pi_p \neq \pi_d, \\ \Delta_j + 1, & \text{for odd } \Delta_j \text{ and } \pi_p = \pi_d. \end{cases} \quad (9)$$

Here, $\Delta_j = |j_p - j_d - j_{proton}|$, where j_p, π_p, j_d, π_d, j_{proton}, and π_{proton} are the spin and parity values for parent, daughter, and proton, respectively. In addition, when a proton is separated from the parent nucleus, the Coulomb potential $V_c(r)$ is expressed as

$$V_c(r) = \frac{Z_{proton}Z_d e^2}{r}. \quad (10)$$

To describe the process of proton radioactivity, we employed the Hulthen-type potential instead of the Coulomb potential, which causes the superposition of the involved charges, movement of the emitted proton (which generates a magnetic field), and an inhomogeneous charge distribution in the nucleus. It can be defined as

$$V_h(r) = \frac{tZ_{proton}Z_d e^2}{e^{tr} - 1}, \quad (11)$$

where e^2=1.4399652 MeV·fm and t is the screened parameter. In fact, the Hulthen-type potential is a generation of Coulomb potential. At short distances, its behavior is very similar to that of the Coulomb potential; however, at large distances, it drops exponentially. To intuitively show the difference between the Coulomb potential and Hulthen potential at large distances, Fig. 2 displays a schematic diagram of interaction potential in a separating region, taking the process of proton radioactivity of nucleus ^{146}Tm as an example. It can be concluded from this figure that with an increase in r, the error between the Coulomb potential and Hulthen

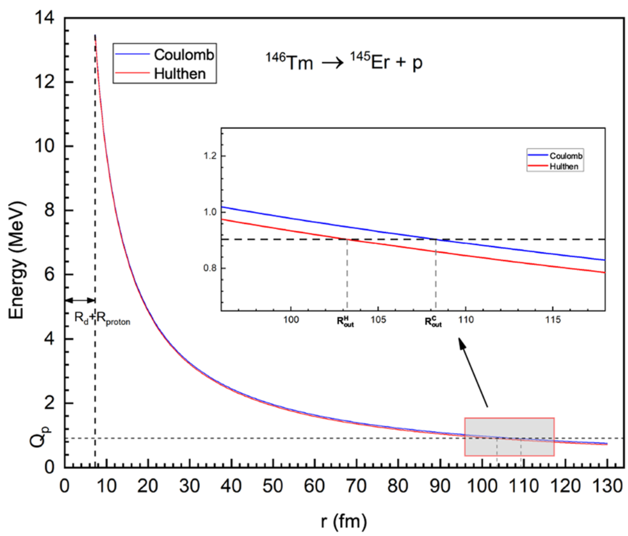

Fig. 2 (Color online) Schematic diagram of proton-^{145}Er nucleus Coulomb potential and Hulthen potential in the separating region

potential increases. Meanwhile, the Hulthen potential shifts the outer turning point to the left.

In the overlapping region, the reduced mass and interaction potential cannot be treated as a free two-body system, because the proton is not completely separated from the parent nucleus. Here, we use μ_{ov} and $V(r)_{ov}$ to represent the reduced mass and interaction potential in this region, respectively. Inspired by Refs. [59, 60], they can be expressed as

$$\mu_{ov} = \mu_0\left(\frac{r-a}{b-a}\right)^p, \quad p \geq 0\,, \tag{12}$$

$$V_{ov}(r) = Q_p + \left(V(b) - Q_p\right)\left(\frac{r-a}{b-a}\right)^q, \quad q \geq 1, \tag{13}$$

with

$$V(b) = V_h(b) + V_l(b) = \frac{tZ_{proton}Z_d e^2}{e^{tb}-1} + \frac{(l+1/2)^2\hbar^2}{2\mu_0 b^2}. \tag{14}$$

According to Eqs. (3, 12, and 13), the expression for G_{ov} can be rewritten as

$$G_{ov} = 0.4374702(b-a)\left(1+\frac{p+q}{2}\right)^{-1} \left\{\mu_0\left[\frac{tZ_{proton}Z_d e^2}{e^{tb}-1} + \frac{20.9008(l+1/2)^2}{\mu_0 b^2} - Q_p\right]\right\}^{1/2}, \tag{15}$$

where $(1+\frac{p+q}{2})^{-1}$ is denoted by g, with $0 \leq g \leq \frac{2}{3}$. The parameter g encodes an adjustable coupling of the mass power parameter p and potential energy power parameter q. It represents the combined effect of the interaction potential and reduced mass of the proton-daughter nucleus on the half-life of proton radioactivity in the overlapping region. Once a proton is separated from the parent nucleus, the proton radioactivity system becomes a simple two-body problem. The reduced mass μ_{se} can be obtained using Eq. (4), i.e., μ_0; meanwhile, the potential energy $V_{se}(r)$ includes the Hulthen-type and centrifugal potentials. Therefore, G_{se} can be expressed as

$$G_{se} = 0.62994397 Z_d\left(\frac{\mu_0}{Q_p}\right)^{1/2} \times F, \tag{16}$$

where

$$\begin{aligned} F = &\frac{x^{1/2}}{2y} \times \ln\left\{\frac{\left[x(x+2y-1)\right]^{1/2} + x + y}{(x/y)\left[1+(1+x/y^2)^{1/2}\right]^{-1} + y}\right\} \\ &+ \arccos\left\{\frac{1}{2}\left[1 - \frac{1-1/y}{(1+x/y^2)^{1/2}}\right]\right\}^{1/2} \\ &- \left[\frac{1}{2y}(1+x/2y-1/2y)\right]^{1/2}, \end{aligned} \tag{17}$$

with

$$\begin{aligned} x &= \frac{20.9008(l+1/2)^2}{\mu_0 b^2 Q_p}\,, \\ y &= \frac{\ln\left(tZ_{proton}Z_d e^2/Q_p + 1\right)}{2tb}. \end{aligned} \tag{18}$$

Then, the proton radioactivity half-life can be calculated by

$$T_{1/2} = 4.108054431 \times 10^{-23}\frac{\mu_0 R_0{}^2}{G+3/2} S_p{}^{-1} P_{se}{}^{-1}. \tag{19}$$

3 Results and discussion

On the basis of the Gamow model, replacing the Coulomb potential with the Hulthen-type potential, an improved model is proposed to investigate the half-lives of proton radioactivity. We selected 45 proton emitters with $51 \leq Z \leq 83$ as the database and divided them into 32 spherical nuclei and 13 deformed nuclei. For spherical nuclei, using a genetic algorithm with the optimal solution of σ as the objective function, we obtained the values of the adjustable parameters: t=9.186×10^{-4} and g=4.313×10^{-3}. In this study, σ, i.e., the deviation between the experimental and calculated data, is defined as

$$\sigma = \sqrt{\sum(\log_{10}T_{1/2}^{cal} - \log_{10}T_{1/2}^{exp})^2/n}, \tag{20}$$

where $\log_{10}T_{1/2}^{\mathrm{cal}}$ and $\log_{10}T_{1/2}^{\mathrm{exp}}$ are the experimental and calculated proton radioactivity half-lives in logarithmic form, and n denotes the number of nuclei involved in each case.

To visualize the screened electrostatic effect, Fig. 3 shows the difference between the outer turning points before and after considering the screened effect versus $Z_\mathrm{d}/Q_\mathrm{p}$. $R_{\mathrm{out}}^{\mathrm{H}}$ and $R_{\mathrm{out}}^{\mathrm{C}}$ represent the outer turning points obtained by the Gamow model with Hulthen-type and Coulomb potentials, respectively. According to this figure, it can be concluded that the screening of electrostatic repulsion shortens the outer turning point by several percentage points, but we also conclude that the larger the ratio $Z_\mathrm{d}/Q_\mathrm{p}$, the more evident this effect is for the penetrability factor.

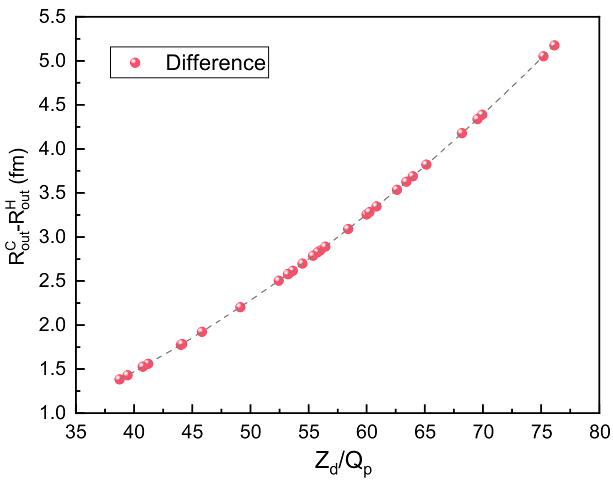

Fig. 3 (Color online) Difference between $R_{\mathrm{out}}^{\mathrm{C}}$ and $R_{\mathrm{out}}^{\mathrm{H}}$ obtained by the proposed improved Gamow model, where the electrostatic barrier is dismissed and considered, respectively. The turning point radii are defined as $V_i(R_{\mathrm{out}}^i)=Q_\mathrm{p}$ (i=C, H)

Using the proposed improved Gamow model and the obtained values of the parameters t and g, we calculated the proton radioactivity half-lives of 32 spherical nuclei. Detailed calculations are presented in Table 1. In this table, the first two columns present the proton emitter and corresponding energy released by proton radioactivity, Q_p, respectively. The next two columns denote the spin and parity transition and the minimum angular momentum removed by the emitted proton l_{min}, respectively. The last four columns are the half-lives of the experimental proton radioactivity, half-lives calculated using the proposed improved model, UDLP, and NG-N, all expressed in logarithmic form as $\log_{10}T_{1/2}^{\mathrm{exp}}$, $\log_{10}T_{1/2}^{\mathrm{cal}}$, $\log_{10}T_{1/2}^{\mathrm{UDLP}}$, and $\log_{10}T_{1/2}^{\mathrm{NG-N}}$, respectively. It can be easily seen from this table that the calculations from the proposed model are very close to the experimental values for all nuclei except for $^{177}\mathrm{Tl}^{\mathrm{m}}$, whose calculated half-life differs by approximately one order of magnitude from the experimental value. Furthermore, the total rms deviation for spherical nuclei calculated by our model is 0.331 orders of magnitude and decreases to 0.274 when $^{177}\mathrm{Tl}^{\mathrm{m}}$ is not considered. For comparison, Table 2 lists the standard deviations σ calculated within 31 spherical nuclei (except for $^{177}\mathrm{Tl}^{\mathrm{m}}$), NG-N, and UDLP. The results show that the calculated proton radioactivity half-lives of spherical nuclei are reliable.

To intuitively demonstrate the consistency between our results and the experimental data, Fig. 4a shows the differences between the experimental half-lives of proton radioactivity and the calculated half-lives in logarithmic form for spherical proton emitters using the proposed improved Gamow model, NG-N, and UDLP. They are represented by

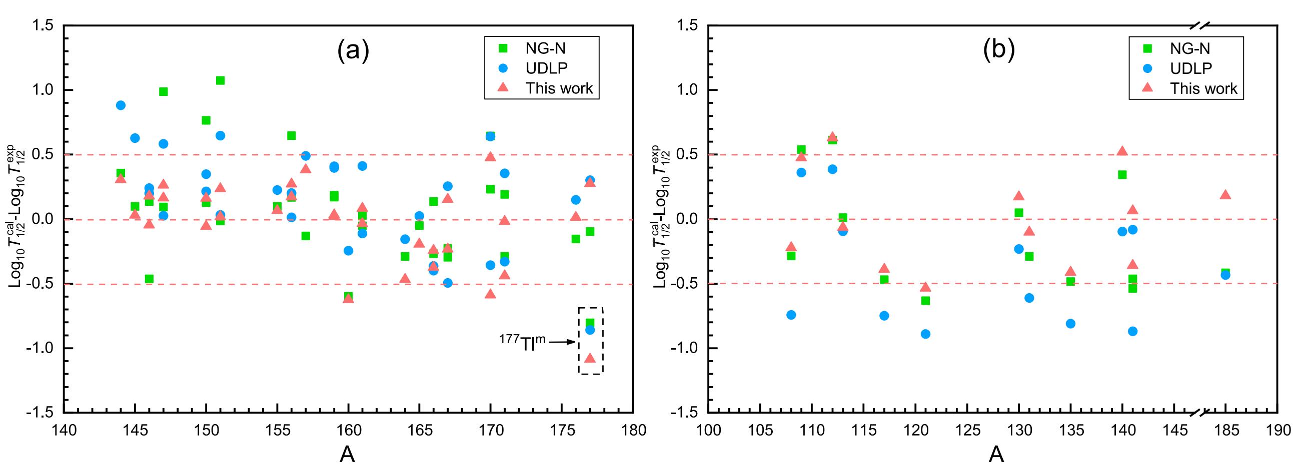

Fig. 4 (Color online) Deviations between the experimental proton radioactivity half-lives and corresponding calculated half-lives in logarithmic form for spherical **a** and deformed **b** nuclei. The red triangle, green square, and blue circle represent the deviations calculated by the proposed improved Gamow model, NG-N, and UDLP, respectively

red triangle, green square, and blue circle, respectively. As can be seen from this figure, compared with the calculations using the other two formulas, our results are generally closer to the experimental values. The deviations of most of the spherical nuclei are within 0.5. This indicates that our model can reproduce the experimental half-lives accurately. The exception is ^{177}Tl^{m}, for which the agreement with the experimental data is worse for the improved Gamow model, NG-N, and UDLP, with corresponding deviations of −1.084, −0.802, and −0.859, respectively. The reason for this large discrepancy is worth investigating. Given that our calculations are determined by two experimental quantities, i.e., the energy released by proton radioactivity Q_{p} and the angular momentum l, Fig. 5 presents the proton radioactivity half-lives of ^{177}Tl^{m} calculated by our model in logarithmic form versus Q_{p}. The dotted lines with different colors correspond to the proton radioactivity half-lives with different angular momenta l whereas the red spheres represent the experimental data of ^{177}Tl^{m}. According to this figure, we can conclude that the results are sensitive to l whereas the dependence on Q_{p} is not so pronounced. For the same decay energy, the half-lives increase by an order of magnitude or more for each increase in angular momentum. Moreover, the experimental data perfectly fit on the line with $l = 6$, which is larger than that of experimental $l = 5$. The same phenomenon was reported by A. Zdeb et al. [54]. They analyzed the single-particle energies from microscopic calculations using the Hartree Fock-Bogolubow model with the Gogny-type force D1S parameter set of ^{177}Tl^{m}. It can be concluded that the first $l = 6$ state $13/2^{+}$ is approximately 9.5 MeV above the $1/2^{+}$ ground state, and that the angular momentum $l = 6$ cannot be associated with ^{177}Tl^{m}, which has an excitation energy of only 807 keV. However, the experimental data of spin and parity for ^{177}Tl^{m} in NUBASE2020 are uncertain. According to the proton radioactivity satisfying the conservation law of spin and parity, this leads to an uncertain value of l removed by the emitted proton. Thus, in our opinion, the orbital angular momentum of ^{177}Tl^{m} may be $l = 6$.

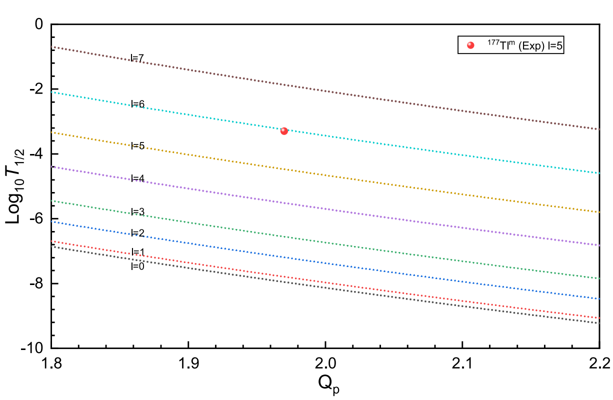

Fig. 5 (Color online) Q_{p} dependence of the proton radioactivity half-lives for ^{177}Tl^{m} with various angular momenta (l_{exp}=5)

Recently, the study of deformed nuclei has attracted extensive attention [55, 56]. Therefore, it would be interesting to extend our model to deformed nuclei. Theoretically, the probability of proton formation depends on deformation of the decaying nucleus. In a well-deformed nucleus, decay can proceed through one of the spherical components of the deformed orbit, which can be very small in case of large deformations. Thus, the probability of formation is small. Using our model with the parameters fitted from the spherical nuclei to calculate 13 deformed nuclei, we found that the calculated results were not in satisfactory agreement with the experimental values. The error of several nuclei reached an order of magnitude. This phenomenon is probably due to the deformation effect that affects the total potential energy and some other factors, such that the probabilities of finding a proton at the nuclear surface S_{p} and a proton penetrating through the external barrier P_{se} vary with respect to those of spherical nuclei. Using the experimental data of 13 deformed nuclei as a database, we obtained a new set of parameters, i.e., t=1.831×10^{-4} and g=0.666, by refitting. It is worth noting that the values of t for the deformed and spherical nuclei are the same in magnitude, whereas g for the spherical nuclei is close to zero and for the deformed nuclei is greater than 0.5. This difference in the g value directly affects S_{p}; thus, the corresponding S_{p} values became 0.98 and 0.17 on average for spherical and deformed nuclei, respectively. This suggests that spherical nuclei have narrower overlapping regions than deformed nuclei, and that protons are more likely to escape the spherical parent nucleus. The relevant results and deviations are displayed in Part II of Table 1 and subfigure b in Fig. 4, respectively; note that the calculations agree well with the experimental data. Generally, the advantage of our model is that it avoids direct consideration of the complex nuclear potential and Coulomb potential in the overlapping region. Besides, it uses a single parameter to characterize the influence of the physical quantity of the overlapping region on the proton radioactivity half-life. We fitted different parameter values for deformed and spherical nuclei and systematically studied the effect of deformation on the spectroscopic factor S_{p} and half-life of the proton radioactivity. Nevertheless, by fitting the adjustable parameters through experimental data, the physical meaning of our model is not as clear as that of microscopic models when considering the effect of deformation on the half-life of proton radioactivity.

In the following, we extend our improved Gamow model to predict the proton radioactivity half-lives of 18 nuclei, whose proton radioactivity is energetically allowed or observed but not yet quantified in NUBASE2020. For

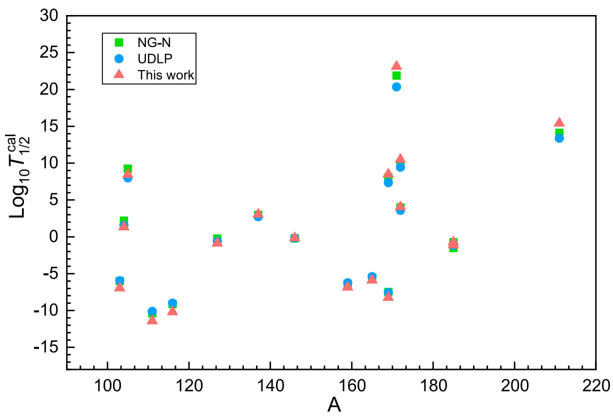

Fig. 6 (Color online) Comparison of the predicted proton radioactivity half-lives using our model, NG-N, and UDLP. They are denoted by red triangle, green square, and blue circle, respectively

comparison, UDLP and NG-N were also used. The predicted proton radioactivity half-lives are listed in Table 3. For a more visual comparison, the predictions of the three models are plotted in Fig. 6. The results show that the values predicted by UDLP, NG-N, and our model are consistent. To further verify the reliability of our predictions, we plotted the relationships between the logarithm of experimental and predicted half-lives and $Z_{\mathrm{d}}^{0.8}/Q_{\mathrm{p}}^{1/2}$, i.e., the new Geiger-Nuttall law [42] for proton radioactivity, for l=0, 2, 3, and 5; the results are depicted in Fig. 7. The dashed lines in this figure were fitted to the experimental data. From this figure, we can clearly see that our predicted proton radioactivity half-lives fit the linear relevance well. This indicates that our predicted results may be useful for future studies on proton emission half-lives in newly synthesized isotopes.

4 Summary

In summary, based on the Gamow model and considering the screened electrostatic effect, we systematically studied proton radioactivity half-lives. The calculated results show that the experimental data for both spherical and deformed nuclei can be reproduced well with

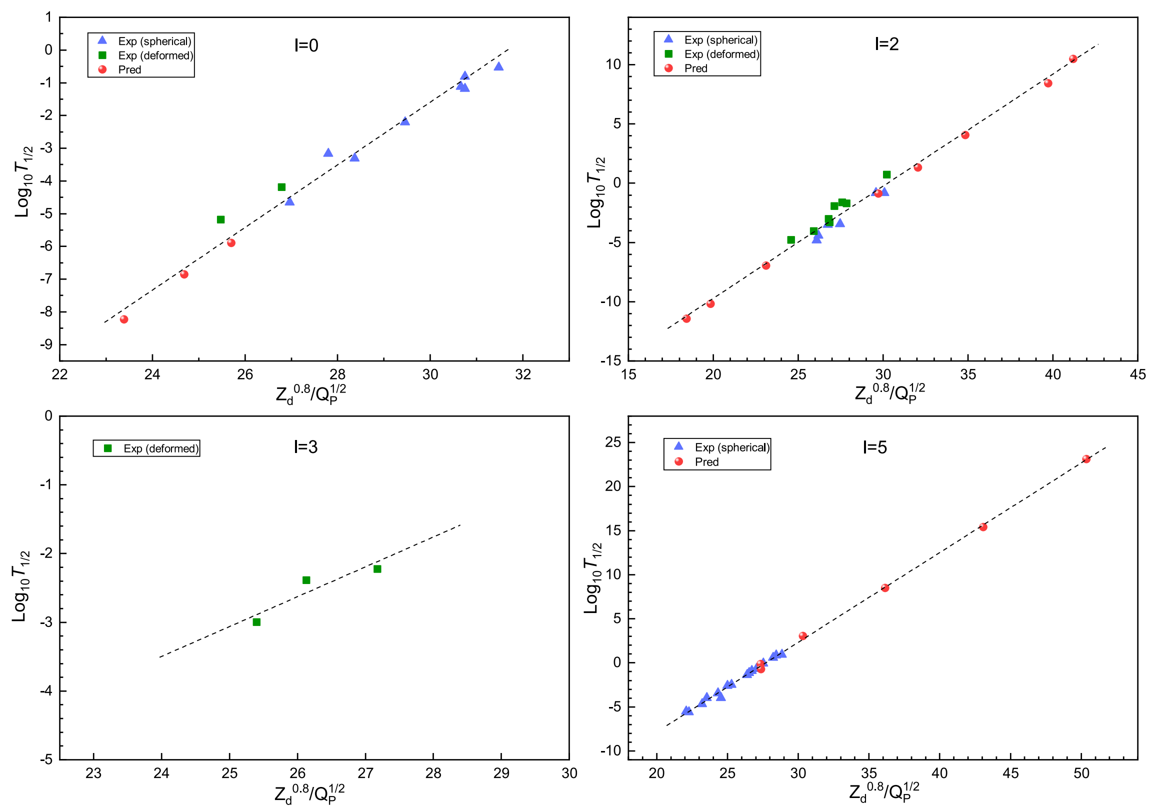

Fig. 7 (Color online) Logarithmic values of the experimental half-lives and predicted half-lives versus $Z_{\mathrm{d}}^{0.8}/Q_{\mathrm{p}}^{1/2}$ for l=0, 2, 3, 5. The blue triangle, green square, and red sphere denote the experimental proton radioactivity half-lives of spherical and deformed nuclei, and predicted half-lives, respectively

Table 1 Proton radioactivity half-lives in logarithmic form calculated by our improved Gamow model, NG-N, and UDLP. The experimental proton emission half-lives, spin, and parity were taken from the latest table of evaluated nuclear properties, i.e., NUBASE2020 [51]. The values of Q_p were taken from the latest table of evaluated atomic masses, i.e., AME2020 [61, 62]. The proton emission energy and half-lives are expressed in MeV and s, respectively

Nucleus	Q_p	$j_p^\pi \to j_d^\pi$	l	$\log_{10}T_{1/2}^{exp}$	$\log_{10}T_{1/2}^{cal}$	$\log_{10}T_{1/2}^{NG-N}$	$\log_{10}T_{1/2}^{UDLP}$
Part I: Spherical nuclei							
^{144}Tm	1.724	$(10^+) \to 9/2^-$#	5	−5.569	−5.263	−5.212	−4.687
^{145}Tm	1.754	$(11/2^-) \to 0^+$	5	−5.499	−5.467	−5.401	−4.871
^{146}Tm	0.904	$(1^+) \to (1/2^+)$	0	−0.810	−0.854	−1.272	−0.610
^{146}Tm^m	1.214	$(5^-) \to (1/2^+)$	5	−1.137	−0.959	−0.999	−0.896
^{147}Tm^m	1.133	$3/2^+ \to 0^+$	2	−3.444	−3.181	−2.455	−2.859
^{147}Tm	1.072	$11/2^- \to 0^+$	5	0.587	0.752	0.681	0.614
^{150}Lu^m	1.305	$(1+,2^+) \to (1/2^+)$	2	−4.398	−4.454	−3.633	−4.050
^{150}Lu	1.285	$(5^-) \to (1/2^+)$	5	−1.347	−1.186	−1.219	−1.132
^{151}Lu^m	1.315	$3/2^+ \to 0^+$	2	−4.796	−4.561	−3.722	−4.150
^{151}Lu	1.255	$11/2^- \to 0^+$	5	−0.896	−0.877	−0.910	−0.862
^{155}Ta	1.466	$11/2^- \to 0^+$	5	−2.495	−2.427	−2.397	−2.269
^{156}Ta	1.036	$(2^-) \to 7/2^-$#	2	−0.826	−0.654	−0.180	−0.624
^{156}Ta^m	1.126	$(9^+) \to 7/2^-$#	5	0.933	1.205	1.101	0.947
^{157}Ta	0.946	$1/2^+ \to 0^+$	0	−0.527	−0.145	−0.657	−0.038
^{159}Re^m	1.816	$11/2^- \to 0^+$	5	−4.665	−4.646	−4.494	−4.269
^{159}Re	1.816	$11/2^- \to 0^+$	5	−4.678	−4.645	−4.493	−4.268
^{160}Re	1.267	$(4^-) \to 7/2^-$#	0	−3.163	−3.786	−3.761	−3.408
^{161}Re	1.216	$1/2^+ \to 0^+$	0	−3.306	−3.223	−3.277	−2.895
^{161}Re^m	1.336	$11/2^- \to 0^+$	5	−0.678	−0.712	−0.729	−0.789
^{164}Ir	1.844	$(9^+) \to 7/2^-$	5	−3.959	−4.426	−4.247	−4.114
^{165}Ir^m	1.727	$(11/2^-) \to 0^+$	5	−3.433	−3.626	−3.482	−3.408
^{166}Ir	1.167	$(2)^- \to (7/2^-)$	2	−0.824	−1.198	−0.688	−1.188
^{166}Ir^m	1.347	$(9)^+ \to (7/2^-)$	5	−0.076	−0.318	−0.344	−0.475
^{167}Ir	1.087	$1/2^+ \to 0^+$	0	−1.120	−0.967	−1.347	−0.865
^{167}Ir^m	1.262	$11/2^- \to 0^+$	5	0.842	0.611	0.546	0.348
^{170}Au	1.487	$(2)^- \to (7/2^-)$	2	−3.487	−4.074	−3.254	−3.845
^{170}Au^m	1.767	$(9)^+ \to (7/2^-)$	5	−3.975	−3.499	−3.330	−3.333
^{171}Au	1.464	$1/2^+ \to 0^+$	0	−4.652	−4.669	−4.460	−4.298
^{171}Au^m	1.702	$11/2^- \to 0^+$	5	−2.587	−3.025	−2.876	−2.915
^{176}Tl	1.278	$(3^-,4^-) \to (7/2^-)$	0	−2.208	−2.194	−2.361	−2.059
^{177}Tl	1.173	$(1/2^+) \to 0^+$	0	−1.178	−0.901	−1.274	−0.875
^{177}Tl^m	1.963	$(11/2^-) \to 0^+$	5	−3.346	−4.431	−4.148	−4.205
Part II: Deformed nuclei							
^{108}I	0.610	(1^+)# $\to 5/2^+$#	2	0.723	0.502	0.438	−0.019
^{109}I	0.829	$(3/2^+) \to 0^+$	2	−4.032	−3.558	−3.493	−3.671
^{112}Cs	0.820	1^+# $\to 5/2^+$#	2	−3.310	−2.681	−2.697	−2.923
^{113}Cs	0.978	$(3/2^+) \to 0^+$	2	−4.771	−4.836	−4.760	−4.865
^{117}La	0.823	$(3/2^+) \to 0^+$	2	−1.602	−1.991	−2.072	−2.350
^{121}Pr	0.901	$(3/2^+) \to 0^+$	2	−1.921	−2.456	−2.552	−2.811
^{130}Eu	1.028	$(1^+) \to (1/2^+,3/2^+)$	2	−3.000	−2.828	−2.950	−3.233
^{131}Eu	0.951	$3/2^+ \to 0^+$	2	−1.699	−1.800	−1.988	−2.310
^{135}Tb	1.203	$(7/2^-) \to 0^+$	3	−2.996	−3.408	−3.479	−3.806
^{140}Ho	1.104	$6^-,0^+,8^+ \to (7/2^+)$	3	−2.222	−1.702	−1.877	−2.317
^{141}Ho^m	1.256	$(1/2^+) \to 0^+$	0	−5.180	−5.115	−5.717	−5.261
^{141}Ho	1.194	$(7/2^-) \to 0^+$	3	−2.387	−2.747	−2.850	−3.257
^{185}Bi^m	1.607	$1/2^+ \to 0^+$	0	−4.191	−4.011	−4.606	−4.623

Table 2 Standard deviations between the experimental proton radioactivity half-lives and calculated half-lives, NG-N, and UDLP for 31 spherical nuclei and 13 deformed nuclei denoted as σ_1, σ_2, and σ_3

Nuclei	σ			
	Cases	σ_1	σ_2	σ_3
Spherical nuclei	31	0.274	0.399	0.385
Deformed nuclei	13	0.367	0.437	0.571

the corresponding parameters. We also analyzed the relationship between the half-life and l of ^{177}Tl^{m}, and propose a possible reference value: l=6. Moreover, we extended this model to predict the proton radioactivity half-lives of 18 nuclei whose proton radioactivity is energetically allowed or observed but not yet quantified in NUBASE2020 and compare them with the predictions of UDLP and NG-N. The results predicted by our model and by these two formulas were consistent with each other. In addition, we verified the reliability of our predictions using the new Geiger-Nuttall law. This study will prompt inquiries regarding nuclear structures and provide information for future experiments.

Table 3 Same as Table 1, but for predicted radioactivity half-lives of nuclei in region 51≤ Z ≤83 in which proton radioactivity is energetically allowed or observed but not yet quantified in NUBASE2020 [51]

Nucleus	Q_p	$j_p^\pi \to j_d^\pi$	l	$\log_{10}T_{1/2}^{exp}$	$\log_{10}T_{1/2}^{cal}$	$\log_{10}T_{1/2}^{NG-N}$	$\log_{10}T_{1/2}^{UDLP}$
Part I: Spherical nuclei							
^{146}Tm^{n}	1.144	$(10^+) \to 11/2^-\#$	5	–	−0.145	−0.206	−0.177
^{159}Re	1.606	$1/2^+\# \to 0^+$	0	–	−6.854	−6.381	−6.227
^{165}Ir	1.547	$1/2^+\# \to 0^+$	0	–	−5.897	−5.530	−5.387
^{169}Ir^{m}	0.782	$(11/2^-) \to 0^+$	5	–	8.499	8.043	7.362
^{171}Ir^{m}	0.403	$(11/2^-) \to 0^+$	5	–	23.122	21.891	20.337
^{169}Au	1.947	$1/2^+\# \to 0^+$	0	–	−8.227	−7.478	−7.572
^{172}Au	0.877	$(2^-) \to 7/2^-$	2	> 0.146	4.070	3.983	3.578
^{172}Au^{m}	0.627	$(9^+) \to 13/2^+$	2	> −0.260	10.497	9.678	9.433
Part II: Deformed nuclei							
^{103}Sb	0.979	$5/2^+\# \to 0^+$	2	–	−6.148	−6.009	−5.948
^{104}Sb	0.509	$() \to 5/2^+\#$	2	> 0.827	2.200	2.187	1.550
^{105}Sb	0.331	$(5/2^+) \to 0^+$	2	> 3.049	9.388	9.240	8.002
^{111}Cs	1.740	$3/2^+\# \to 0^+$	2	–	−10.640	−10.375	−10.094
^{116}La	1.591	$() \to 5/2^+\#$	2	–	−9.375	−9.126	−9.000
^{127}Pm	0.792	$5/2^+\# \to 0^+$	2	–	0.033	−0.239	−0.620
^{137}Tb	0.843	$11/2^-\# \to 0^+$	5	–	4.038	2.974	2.714
^{185}Bi	1.541	$9/2^-\# \to 0^+$	5	–	0.330	−0.732	−1.030
^{185}Bi^{n}	1.721	$13/2^+\# \to 0^+$	6	–	−0.020	−1.512	−1.171
^{211}Pa	0.721	$9/2^-\# \to 0^+$	5	–	16.535	14.099	13.366

Author Contributions All authors contributed to the study conception and design. Material preparation, data collection and analysis were performed by Xiao-Yuan Hu, De-Xing Zhu, Xi-Jun Wu, Peng-Cheng Chu and Xiao-Hua Li. The first draft of the manuscript was written by Yang-Yang Xu, and all authors commented on previous versions of the manuscript. All authors read and approved the final manuscript.

References

1. K.P. Jackson, C.U. Cardinal, H.C. Evans et al., ^{53}Co^{m}: A proton-unstable isomer. Phys. Lett. B **33**, 281 (1970). https://doi.org/10.1016/0370-2693(70)90269-8
2. J. Cerny, J. Esterl, R. Gough et al., Confirmed proton radioactivity of ^{53}Co^{m}. Phys. Lett. B **33**, 284 (1970). https://doi.org/10.1016/0370-2693(70)90270-4
3. S. Hofmann, W. Reisdorf, G. Münzenberg et al., proton radioactivity of ^{151}Lu. Z. Phys. A **305**, 111 (1982). https://doi.org/10.1007/BF01415018
4. O. Klepper, T. Batsch, S. Hofmann et al., Direct and beta-delayed proton decay of very neutron-deficient rare-earth isotopes produced in the reaction ^{58}Ni+^{58}Mo. Z. Phys. A **305**, 125 (1982). https://doi.org/10.1007/BF01415019
5. J.G. Deng, X.H. Li, J.L. Chen et al., Systematic study of proton radioactivity of spherical proton emitters within various versions of proximity potential formalisms. Eur. Phys. J. A **55**, 58 (2019). https://doi.org/10.1140/epja/i2019-12728-0
6. J.H. Cheng, J.L. Chen, J.G. Deng et al., Systematic study of α decay half-lives based on Gamow-like model with a screened electrostatic barrier. Nucl. Phys. A **987**, 350 (2019). https://doi.org/10.1016/j.nuclphysa.2019.05.002
7. L. Zhou, S.M. Wang, D.Q. Fang et al., Recent progress in two-proton radioactivity. Nucl. Sci. Tech. **33**, 105 (2022). https://doi.org/10.1007/s41365-022-01091-1
8. J.H. Cheng, X. Pan, Y.T. Zou et al., Systematic study of proton radioactivity of spherical proton emitters with Skyrme interactions. Eur. Phys. J. A **56**, 273 (2020). https://doi.org/10.1140/epja/s10050-020-00280-z
9. D.X. Zhu, H.M. Liu, Y.Y. Xu et al., Two-proton radioactivity within Coulomb and proximity potential model. Chin. Phys. C **46**, 4 (2022). https://doi.org/10.1088/1674-1137/ac45ef
10. H.C. Manjunatha, N. Sowmya, P.S. Damodara Gupta et al., Investigation of decay modes of superheavy nuclei. Nucl. Sci. Tech. **32**, 130 (2021). https://doi.org/10.1007/s41365-021-00967-y
11. D.X. Zhu, Y.Y. Xu, H.M. Liu et al., Two-proton radioactivity of the excited state within the Gamowlike and modified Gamow-like models. Nucl. Sci. Tech. **33**, 122 (2022). https://doi.org/10.1007/s41365-022-01116-9
12. J.H. Cheng, J.L. Chen, J.G. Deng et al., Systematic study of proton emission half-lives within the two-potential approach with Skyrme-Hartree-Fock. Nucl. Phys. A **997**, 121717 (2020). https://doi.org/10.1016/j.nuclphysa.2020.121717
13. J.H. Cheng, Y. Li, T.P. Yu, Systematic study of laser-assisted proton radioactivity from deformed nuclei. Phys. Rev. C **105**, 024312 (2022). https://doi.org/10.1103/PhysRevC.105.024312
14. T. Faestermann, A. Gillitzer, K. Hartel et al., Evidence for proton radioactivity of ^{113}Cs and ^{109}I. Phys. Lett. B **137**, 23 (1984). https://doi.org/10.1016/0370-2693(84)91098-0
15. L. Zhou, D.Q. Fang, Effect of source size and emission time on the p-p momentum correlation function in the two-proton emission process. Nucl. Sci. Tech. **31**, 52 (2020). https://doi.org/10.1007/s41365-020-00759-w
16. R.D. Page, P.J. Woods, R.A. Cunningham et al., Decays of odd-odd N-Z=2 nuclei above ^{100}Sn: the observation of proton radioactivity from ^{112}Cs. Phys. Rev. Lett. **72**, 1798 (1994). https://doi.org/10.1103/PhysRevLett.72.1798
17. K. Livingston, P.J. Woods, T. Davinson et al., Proton radioactivity from ^{146}Tm. The completion of a sequence of four odd-odd proton emitters. Phys. Lett. B **312**, 46 (1993). https://doi.org/10.1016/0370-2693(93)90484-Y
18. Y.Z. Wang, J.P. Cui, Y.H. Gao et al., Two-proton radioactivity of exotic nuclei beyond proton drip-line. Commun. Theor. Phys. **73**, 075301 (2021). https://doi.org/10.1088/1572-9494/abfa00
19. Y.Q. Xin, J.G. Deng, H.F. Zhang, Proton radioactivity within the generalized liquid drop model with various versions of proximity potentials. Commun. Theor. Phys. **73**, 065301 (2021). https://doi.org/10.1088/1572-9494/abf5e6
20. F. Guzmán, M. Gonçalves, O.A.P. Tavares et al., Proton radioactivity from proton-rich nuclei. Phys. Rev. C **59**, R2339(R) (1999). https://doi.org/10.1103/PhysRevC.59.R2339
21. M. Karny, K.P. Rykaczewski, R.K. Grzywacz et al., Shell structure beyond the proton drip line studied via proton emission from deformed ^{141}Ho. Phys. Lett. B **664**, 52 (2008). https://doi.org/10.1016/j.physletb.2008.04.056
22. Ş. Çalışkan, N. Christlieb and K.E. Grebel, Abundance analysis of the outer halo globular cluster Palomar 14. Astron. Astrophys. **537**, A83 (2012). https://doi.org/10.1051/0004-6361/201016355
23. P.J. Sellin, P.J. Woods, T. Davinson et al., Proton spectroscopy beyond the drip line near A=150. Phys. Rev. C **47**, 1933 (1993). https://doi.org/10.1103/PhysRevC.47.1933
24. K. Livingston, P.J. Woods, T. Davinson et al., Isomeric proton emission from the drip-line nucleus ^{156}Ta. Phys. Rev. C **48**, R2151(R) (1993). https://doi.org/10.1103/PhysRevC.48.R2151
25. R.D. Page, P.J. Woods, R.A. Cunningham et al., Discovery of new proton emitters ^{160}Re and ^{156}Ta. Phys. Rev. Lett. **68**, 1287 (1992). https://doi.org/10.1103/PhysRevLett.68.1287
26. D. Rudolph, C. Andreoiu, C. Fahlander et al., Prompt Proton Decay Scheme of ^{59}Cu. Phys. Rev. Lett. **89**, 022501 (2002). https://doi.org/10.1103/PhysRevLett.89.022501
27. Y.B. Qian, Z.Z. Ren, D.D. Ni et al., Half-lives of proton emitters with a deformed density-dependent model. Chin. Phys. Lett. **27**, 112301 (2010). https://doi.org/10.1088/0256-307X/27/11/112301
28. S. Åberg, P.B. Semmes, W. Nazarewicz, Spherical proton emitters. Phys. Rev. C **56**, 1762 (1997). https://doi.org/10.1103/PhysRevC.56.1762
29. M. Bhattacharya, G. Gangopadhyay, Microscopic calculation of half lives of spherical proton emitters. Phys. Lett. B **651**, 263 (2007). https://doi.org/10.1016/j.physletb.2007.06.012
30. D.S. Delion, R.J. Liotta, R. Wyss, Theories of proton emission. Phys. Rep. **424**, 113 (2005). https://doi.org/10.1016/j.physrep.2005.11.001
31. B. Barmore, A.T. Kruppa, W. Nazarewicz et al., Theoretical description of deformed proton emitters: Nonadiabatic coupled-channel method. Phys. Rev. C **62**, 054315 (2000). https://doi.org/10.1103/PhysRevC.62.054315
32. N.C. Davids, H. Esbensen, Particle-vibration coupling in proton decay of near-spherical nuclei. Phys. Rev. C **64**, 034317 (2001). https://doi.org/10.1103/PhysRevC.64.034317
33. M. Balasubramaniam, N. Arunachalam, Proton and α-radioactivity of spherical proton emitters. Phys. Rev. C **71**, 014603 (2005). https://doi.org/10.1103/PhysRevC.71.014603
34. J.M. Dong, H.F. Zhang, W. Zuo et al., Unified fission model for proton emission. Chin. Phys. C **34**, 182 (2010). https://doi.org/10.1088/1674-1137/34/2/005
35. Y.B. Qian, Z.Z. Ren, Calculations on decay rates of various proton emissions. Eur. Phys. J. A **52**, 68 (2016). https://doi.org/10.1140/epja/i2016-16068-3
36. J.M. Dong, H.F. Zhang, G. Royer, Proton radioactivity within a generalized liquid drop model. Phys. Rev. C **79**, 054330 (2009). https://doi.org/10.1103/PhysRevC.79.054330

37. H.F. Zhang, Y.J. Wang, J.M. Dong et al., Concise methods for proton radioactivity. J. Phys. G Nucl. Part. Phys. **37**, 085107 (2010). https://doi.org/10.1088/0954-3899/37/8/085107
38. Y.Z. Wang, J.P. Cui, Y.L. Zhang et al., Competition between α decay and proton radioactivity of neutron-deficient nuclei. Phys. Rev. C **95**, 014302 (2017). https://doi.org/10.1103/PhysRevC.95.014302
39. D.N. Basu, P.R. Chowdhury, C. Samanta, Folding model analysis of proton radioactivity of spherical proton emitters. Phys. Rev. C **72**, 051601 (2005). https://doi.org/10.1103/PhysRevC.72.051601
40. K.P. Santhosh, I. Sukumaran, Description of proton radioactivity using the Coulomb and proximity potential model for deformed nuclei. Phys. Rev. C **96**, 034619 (2017). https://doi.org/10.1103/PhysRevC.96.034619
41. C. Qi, D.S. Delion, R.J. Liotta et al., Effects of formation properties in one-proton radioactivity. Phys. Rev. C **85**, 011303 (2012). https://doi.org/10.1103/PhysRevC.85.011303
42. J.L. Chen, J.Y. Xu, J.G. Deng et al., New Geiger-Nuttall law for proton radioactivity. Eur. Phys. J. A **55**, 214 (2019). https://doi.org/10.1140/epja/i2019-12927-7
43. O.A.P. Tavares, E.L. Medeiros, M.L. Terranovait, Alpha decay half-life of bismuth isotopes. J. Phys. G Nucl. Part. Phys. **31**, 129 (2005). https://doi.org/10.1088/0954-3899/31/2/005
44. O.A.P. Tavares, E.L. Medeiros, M.L. Terranovait, New evaluation of alpha decay half-life of ^{190}Pt isotope for the Pt-Os dating system. Nucl. Instrum. Meth. B **243**, 256 (2006). https://doi.org/10.1016/j.nimb.2005.08.122
45. Y.T. Zou, X. Pan, H.M. Liu et al., Systematic studies on α decay half-lives of neptunium isotopes. Phys. Sci. **96**, 075301 (2021). https://doi.org/10.1088/1402-4896/abf795
46. Y.Y. Xu, D.X. Zhu, Y.T. Zou et al., Systematic study on α-decay half-lives of uranium isotopes with a screened electrostatic barrier. Chin. Phys. C **46**, 114103 (2022). https://doi.org/10.1088/1674-1137/ac7fe8
47. Y.T. Zou, X. Pan, X.H. Li et al., Favored one proton radioactivity within a one-parameter model. Commun. Theor. Phys. **74**, 115302 (2022). https://doi.org/10.1088/1572-9494/ac7e2c
48. L. Hulthen, On the characteristic solutions of the Schrdinger deuteron equation. Ark. Mat. Astron. Fys. A **28**, 52 (1942)
49. J.L. Chen, X.H. Li, J.H. Cheng et al., Systematic study of proton radioactivity based on Gamow-like model with a screened electrostatic barrier. J. Phys. G Nucl. Part. Phys. **46**, 065107 (2019). https://doi.org/10.1088/1361-6471/ab1a56
50. R. Budaca, A.I. Budaca, Proton emission with a screened electrostatic barrier. Eur. Phys. J. A **53**, 160 (2017). https://doi.org/10.1140/epja/i2017-12352-0
51. F.G. Kondev, M. Wang, W.J. Huang et al., The NUBASE2020 evaluation of nuclear physics properties. Chin. Phys. C **45**, 030001 (2021). https://doi.org/10.1088/1674-1137/abddae
52. J.M. Dong, W. Zuo, J.Z. Gu et al., α-decay half-lives and Q_α values of superheavy nuclei. Phys. Rev. C **81**, 064309 (2010). https://doi.org/10.1103/PhysRevC.81.064309
53. W.D. Myers, W.J. Światecki, Nucleus-nucleus proximity potential and superheavy nuclei. Phys. Rev. C **62**, 044610 (2000). https://doi.org/10.1103/PhysRevC.62.044610
54. A. Zdeb, M. Warda, C.M. Petrache et al., Proton emission half-lives within a Gamow-like model. Eur. Phys. J. A **52**, 323 (2016). https://doi.org/10.1140/epja/i2016-16323-7
55. S.Y. Zhong, S.S. Zhang, X.X. Sun et al., Study of the deformed halo nucleus ^{31}Ne with Glauber model based on microscopic self-consistent structures. Sci. China Phys. Mech. **65**, 262011 (2022). https://doi.org/10.1007/s11433-022-1894-6
56. X.Z. Wang, Q.L. Niu, J.J. Zhang et al., Nucleon momentum distribution of ^{56}Fe from the axially deformed relativistic mean-field model with nucleon-nucleon correlations. Sci. China Phys. Mech. **64**, 292011 (2021). https://doi.org/10.1007/s11433-021-1729-5
57. P. Möller, W. D. Myers, W.J. Swiatecki et al., Nuclear mass formula with a finite-range droplet model and a folded-Yukawa single-particle potential. At. Data Nucl. Data Tables **39**, 225 (1988). https://doi.org/10.1016/0092-640X(88)90023-X
58. K.N. Huang, M. Aoyagi, M.H. Chen et al., Neutral-atom electron binding energies from relaxed-orbital relativistic Hartree-Fock-Slater calculations $2 \le Z \le 106$. At. Data Nucl. Data Tables **18**, 243 (1976). https://doi.org/10.1016/0092-640X(76)90027-9
59. S.B. Duarte, M.G. Gonçalves, Effective inertial coefficient for the dinuclear regime of the exotic decay of nuclei. Phys. Rev. C **53**, 2309 (1996). https://doi.org/10.1103/PhysRevC.53.2309
60. D.N. Poenaru, M. Ivaşcu, A. Sndulescu et al., Atomic nuclei decay modes by spontaneous emission of heavy ions. Phys. Rev. C **32**, 572 (1985). https://doi.org/10.1103/PhysRevC.32.572
61. W.J. Huang, M. Wang *et al.*, The AME 2020 atomic mass evaluation (I). Evaluation of input data, and adjustment procedures. Chin. Phys. C **45**, 030002 (2021). https://doi.org/10.1088/1674-1137/abddb0
62. M. Wang, W.J. Huang, F.G. Kondev et al., The AME 2020 atomic mass evaluation (II). Tables, graphs and references. Chin. Phys. C **45**, 030003 (2021). https://doi.org/10.1088/1674-1137/abddaf